

# Xe<sup>+</sup>-Sputtered Molybdenum Properties at Low Impingement Energy

IEPC-2005-194

*Presented at the 29<sup>th</sup> International Electric Propulsion Conference, Princeton University,  
October 31 – November 4, 2005*

Mark W. Crofton<sup>1</sup>

*The Aerospace Corporation, El Segundo, CA, 90245, U.S.A.*

Jonathan C. Murray<sup>2</sup>

*The University of Michigan, Ann Arbor, MI 48109-2140, U.S.A*

*and*

James E. Pollard<sup>3</sup>

*The Aerospace Corporation, El Segundo, CA, 90245, U.S.A.*

**Abstract:** Angle-resolved properties of sputtered molybdenum have been measured for impinging ions with energy below 1 keV. The 0.2 – 1 keV energy range is very relevant for currently operational gridded ion thrusters, and exhibits high dependence on angles of incidence and emission as well as incident energy. To address this problem, the Doppler profiles and relative density of molybdenum atoms sputtered from a small, rotatable target by an independently rotatable ion source were determined by laser-induced fluorescence, the first study of its type for the molybdenum element. The profiles were obtained for various emission angles about the target normal as well as for multiple angles of incidence, and ion impingement energies of 250 and 550 eV. The velocity distributions obtained at each incidence angle, field angle, and beam energy were well-fitted to a Thompson distribution. The fitting-parameter trends are discussed with reference to angles of incidence and emission, and the impingement energy. The most probable kinetic energy of the sputtered particles lies between 2 and 6 eV in each case, and the tail of the distribution extends to much higher values.

## I. Introduction

Sputtering is an indispensable tool in technologies of thin film deposition, surface cleaning and micromachining, generation of ion beams of solid materials, and surface and depth microanalysis. The impact of energetic particles on the surface of a solid leads to ejected particles having a broad angular and energy distribution, with mean energy on the order of 10 eV.<sup>1</sup>

In the sputtering process, the incident ion transfers energy to a “knock-on” atom in excess of the lattice binding energy. This atom is displaced from its original site and loses energy through collisions, just as the incident ion. A collision cascade develops in which other atoms may be removed from their lattice sites, with emission occurring

---

<sup>1</sup> Research Scientist, Propulsion Science and Experimental Mechanics, [mark.w.crofton@aero.org](mailto:mark.w.crofton@aero.org)

<sup>2</sup> Graduate Student, Aerospace Engineering, Email: [murrayjc@engin.umich.edu](mailto:murrayjc@engin.umich.edu)

<sup>3</sup> Senior Scientist, Propulsion Science and Experimental Mechanics, [james.e.pollard@aero.org](mailto:james.e.pollard@aero.org)

when kinetic energy greater than the surface binding energy is imparted to a surface or near-surface atom in the out-bound direction. More than 90% of the ejected atoms originate from the first atomic layer.<sup>2</sup>

For the present situation of Xe<sup>+</sup> bombarding polycrystalline molybdenum, collision cascades will involve just a few atoms if incident energy is low, corresponding to the single knock-on regime. At incident energy of several keV and above, the linear-cascade regime will apply. Each regime will have different characteristics with respect to the emitted atoms, particularly in terms of their total flux and angular distribution and to a lesser degree the kinetic energy distribution. The Xe<sup>+</sup> angle of incidence will also influence the properties of the emitted atoms.

For normal beam incidence the angular flux distributions of atoms sputtered from polycrystalline material are usually close to a cosine function, particularly at medium to high impingement energies. For high-energy impacts of light ions, atoms tend to leave the surface in the normal direction resulting in an over-cosine distribution. For low-energy impacts of massive ions, a larger fraction of the emitted atoms depart at large angles, producing an under-cosine distribution. Non-normal incidence tends to shift the maximum emission away from the incoming direction, but at high incident energy (typically on the order of 100 keV and above) the ejection distribution becomes rotationally symmetric with respect to the surface normal (azimuthally symmetric).

The linear cascade regime normally applies to the approximate range 1-100 keV and leads to distributions that follow the relationship

$$\frac{dY}{d\Omega} \propto \cos^{v_e} \theta_e, \quad 1 \leq v_e < 2 \quad (1)$$

where  $dY/d\Omega$  is the differential sputter yield and  $\theta_e$  is the polar angle of the emitted particle. For over-cosine distributions  $v_e > 1$  and for under-cosine distributions  $v_e < 1$ ; only the former are normally observed in this energy range. Equation (1) is independent of the angle of incidence  $\theta_i$ , except for glancing angles. At energies above 100 keV  $\theta_i$  can be as large as 80° without affecting the emission distribution.

Operational ion thrusters currently use grids made of molybdenum, although carbon grids are projected to become the material of choice. Two previous direct measurements of plume molybdenum have been reported.<sup>3,4</sup> Both studies used relatively low-resolution laser sources so that velocity information was not obtained. Studies of absolute mass deposition rate as a function of plume location have also been performed, using a quartz crystal microbalance (QCM).<sup>5</sup> Although other material also contributes to the QCM signal, an estimate of angular molybdenum flux can be obtained. However, for any measurement situation involving a large-diameter grid, impinging ions with a wide distribution of energy and angle of incidence, and downstream probe location such that sputtered material from across the grid contributes to the signal, measured results represent averages of distributions. The averages themselves may vary somewhat over time; as grids wear the geometry and surface character changes. When surface contamination layers exist, effective sputter yields are modified as well.

Sputtering rates often depend strongly on the impingement energy and angle of incidence. The outgoing flux of material also can depend strongly on the exit angle. Not all of the sputtered material is in the form of neutral atoms – ions and atom clusters are also produced, with proportions subject to conditions. At impingement energies  $\geq 10$  keV, mass flux of clusters may become important. The laser-induced fluorescence measurement does not detect clusters of atoms or ionized species, as the laser frequency coincided with a specific resonance of the neutral atom. Clustering can be safely neglected in the present case due to low impingement energy and allowable error margins.

The integral sputter yield of molybdenum is accurately known as a function of energy. However, few data have been available regarding the differential sputter yield, i.e. the sputter yield per steradian at arbitrary exit angles and its dependence on the angle and energy of incidence. A very recent study used a rotating quartz crystal microbalance to measure the differential sputter yield at 1, 5, and 10 keV impingement energy for several angles of incidence.<sup>6</sup> At both 5 and 10 keV, the differential sputter yield approximates an over-cosine distribution regardless of the angle of incidence. At 1 keV the differential sputter yield distribution is more complex, with weak “butterfly” character and forward sputtering behavior for mid-range angles of incidence and approximately cosine behavior at normal incidence. The region of 300 – 1000 eV is critical, since much of the grid impingement is thought to occur in this range, and the angular flux distributions were found in the present study to be dramatically under-cosine or “butterfly” in character. The relative flux and molybdenum velocity distributions were determined at 250 and 550 eV impingement energies for a series of incidence and exit angles, with a few data also obtained for 1200 eV impingement energy but not discussed in this report.

## II. Experimental

A 3-cm-diameter ion source (Commonwealth Scientific) provided a broad beam of ions to sputter atoms from a small molybdenum target. A single cryopump was used to maintain vacuum, due to the modest xenon flow requirement of the ion source. At the nominal setting of 0.25 mg/s, the facility pressure was  $1 \times 10^{-6}$  Torr. The ion energy was adjustable up to 1500 eV. Ion beam current was 9.5 mA at the 550V setting and 6.0 mA at 250V. A single tungsten filament spanning the molybdenum grids just downstream served to neutralize the ion beam. During normal operation, visible light emission from the filament was intense. The density contribution of sputtered grid material at the probe location was negligible. The ion source and target were independently rotatable with a shared axis of rotation. The effective target dimensions were 1 cm  $\times$  1 cm, and the separation between target and ion source (exit plane of grids) was fixed at 19 cm.

The spectrometer was based on a high resolution, tunable ring dye laser pumped by the ultraviolet output of an argon ion laser. About 6 Watts of uv power excited the Exalite 392E dye to generate laser output at approximately 390 nm. Intracavity elements selected for single frequency operation, and a cavity stabilization system reduced frequency jitter and locked the frequency with respect to an external reference. The resulting frequency bandwidth was  $\leq 1$  MHz, very small in comparison to the molybdenum Doppler width of roughly 10 GHz. The laser frequency was tunable in a single frequency scan up to approximately 30 GHz ( $1.0 \text{ cm}^{-1}$ ), not always adequate to obtain the full Doppler profile. Laser power was on the order of 10 mW, and did not cause significant power broadening or saturation effects.

Small portions of the laser beam were split off to wavemeter and spectrum analyzer instruments. These determined laser frequency and frequency displacement, respectively. The wavemeter accuracy was not sufficient to determine the laser frequency by itself. The spectrum analyzer, a Fabry Perot interferometer with  $0.0500 \text{ cm}^{-1}$  spacing between fringes, was utilized for measurement of relative frequency within laser scans.

The molybdenum transition originated from the lowest electronic energy level, with electron configuration  $4d^5 ({}^6S)5s$  and term  $a^7S (J=3)$ . The electron configuration of the excited state was  $4d^5 ({}^6S)5p$  with term  $z^7P^o (J=2)$ . The transition energy listed in the NIST atomic spectra database is  $25614.367 \text{ cm}^{-1}$ .<sup>7</sup>

The position of the molybdenum transition, with zero Doppler shift, was determined accurately through the use of a reference cell. A small portion of the laser beam was split off and transmitted through the cell. Tripled YAG laser pulses of roughly 20 mJ energy and 10 ns duration (at 355 nm) were focused on a molybdenum surface to generate vapor-phase molybdenum atoms in a helium background (0.5 torr). Fluorescence was monitored using a collection lens, 390-nm bandpass filter and photomultiplier tube.

The remainder of the  $\sim 2$ -mm-diameter laser beam was passed several mm above the target, and the target-to-probe distance was 7.5 cm, large compared to the target dimensions. The angular extent of the target viewed from the probe location could therefore be neglected. Fluorescence was monitored using a spherical collection mirror below the probe region, a lens to focus collected fluorescence into a 0.125-m monochromator, 390-nm bandpass filter and photomultiplier tube.

The fluorescence signal was normalized according to laser power. Relative density was obtained by integrating over the Doppler profiles, and relative flux by integrating the product of velocity and density over the same profiles. The full-width-half-maximum and peak position was determined for each velocity profile to explore angular trends.

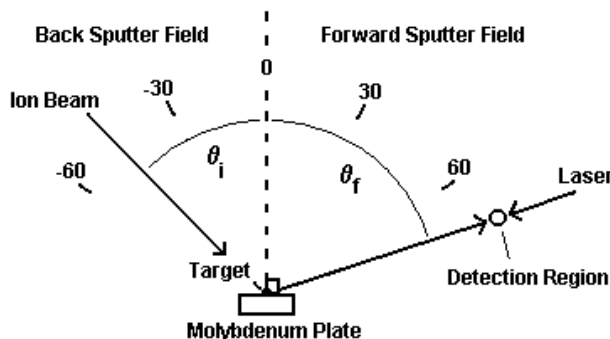


Figure 1. Definition of incidence and field angles.

Velocity distributions of molybdenum atoms sputtered from the target were obtained for many different field (emission) angles about the target normal, various ion beam incidence angles and beam energies of 550V and 250V. Figure 1 shows the definition of the field angle,  $\theta_f$ , and incidence angle,  $\theta_i$ , used in the experiment, as well as the definition of the forward sputter field with respect to the ion beam.

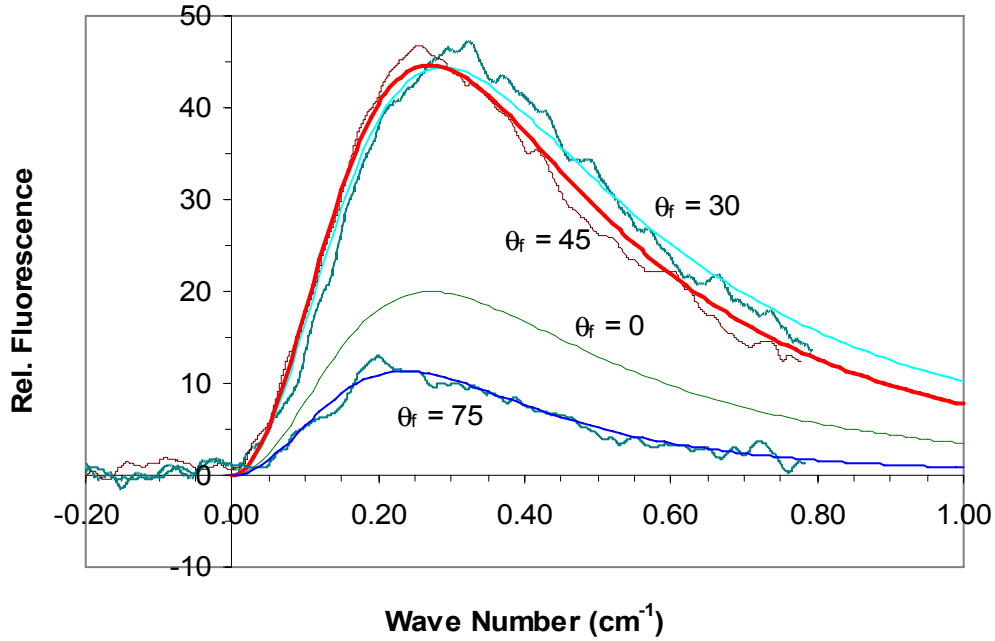


Figure 2. Velocity distribution data and curve fits for  $\theta_i = -70^\circ$  and beam energy of 550 eV.

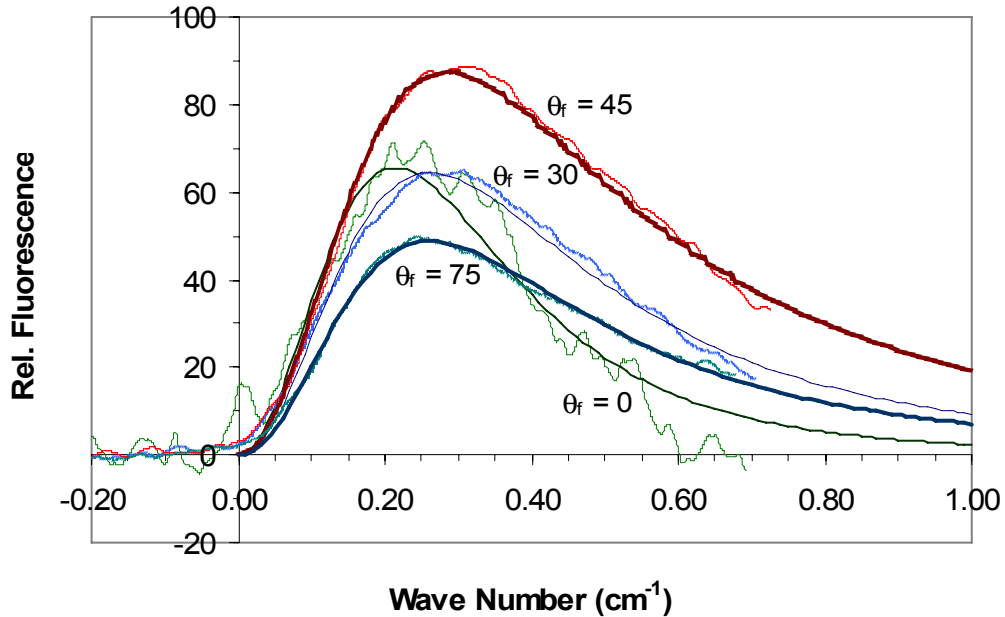


Figure 3. Velocity distribution data and curve fits for  $\theta_i = -30^\circ$  and beam energy of 550 eV.

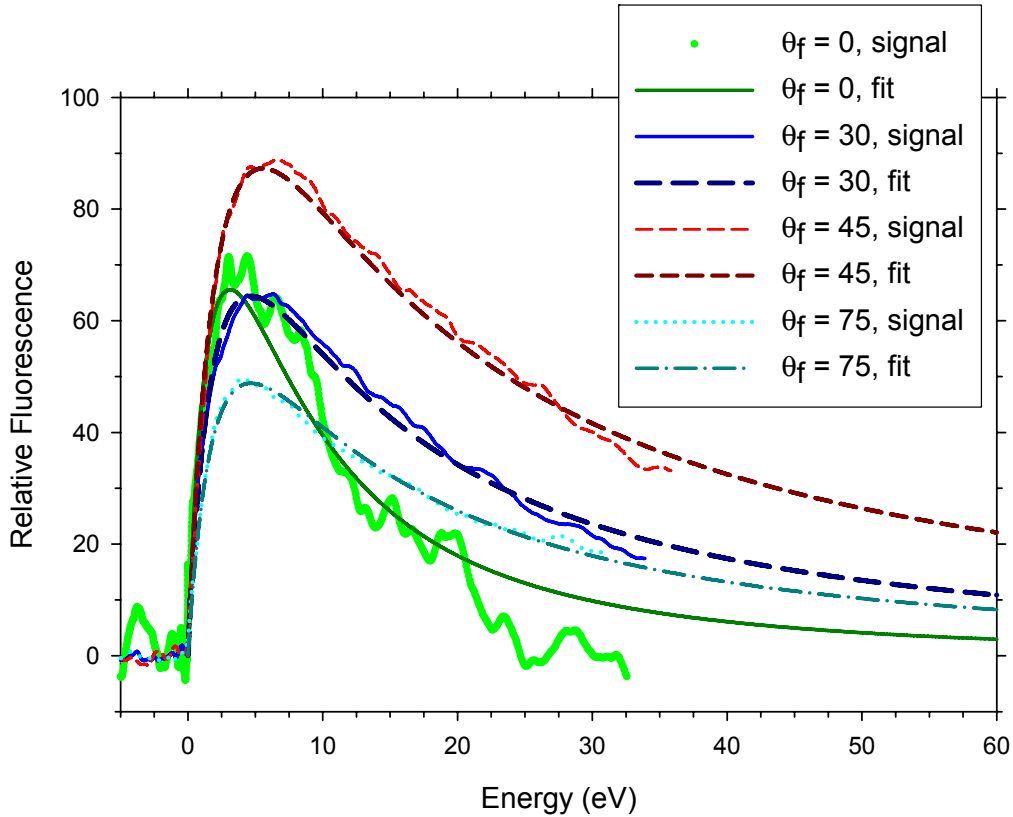


Figure 4. Energy distribution data and curve fits for  $\theta_i = -30^\circ$  and beam energy of 550 eV.

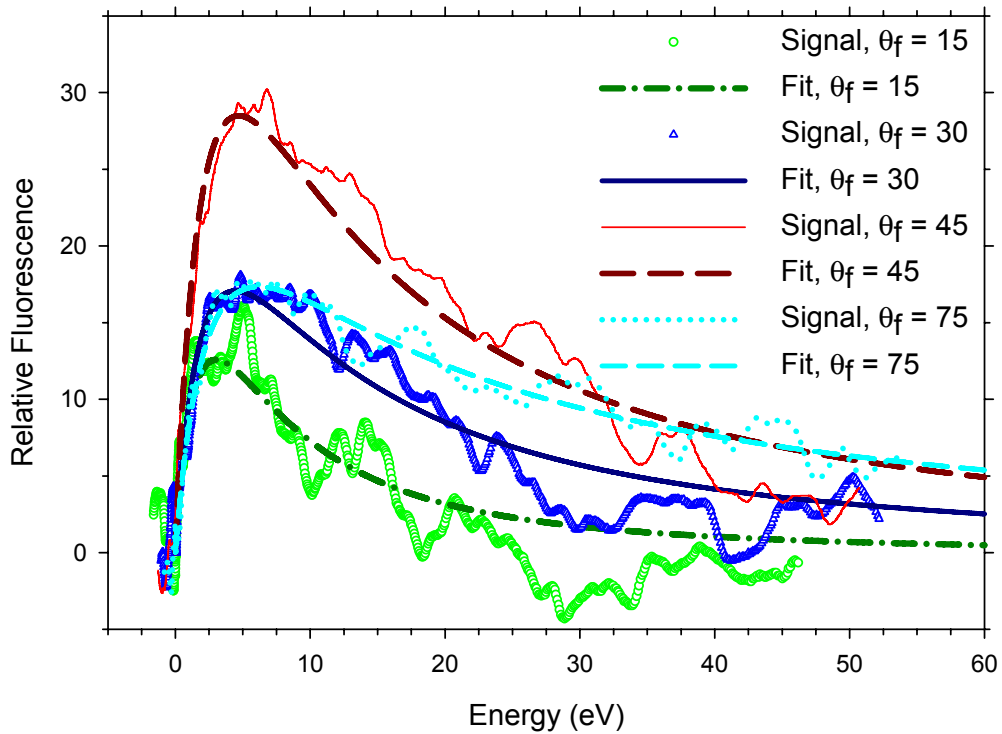


Fig 5. Energy distribution data and curve fits for  $\theta_i = -30^\circ$  and beam energy of 250 eV.

### III. Results and Discussion

The distributions obtained for each incident angle, exit or field angle, and beam energy were fitted to a Thompson distribution of the form<sup>8</sup>

$$\Gamma = \frac{b\nu^2}{(\nu^2 + \nu_b^2)^N} \quad (2)$$

where  $\Gamma$  is the relative density of particles at a velocity corresponding to a measured wave number Doppler shift  $\nu$ . Sputter data have been fit to a Thompson distribution in other studies (see, for example Refs. 9-13). The parameters  $b$  and  $N$  in Eq. 2 are free parameters that were varied to fit the data at each field angle, incidence angle, and energy. The parameter  $\nu_b$  is the Doppler shift, in wavenumbers, that corresponds to the material binding velocity. The material binding velocity,  $V_b$ , is related to the surface binding energy, or heat of sublimation, as

$$V_b = \sqrt{2E_b/M} \quad (3)$$

where  $E_b$  is the surface binding energy and  $M$  is the molecular mass of the particle being sputtered. For molybdenum the surface binding energy is 6.8258 eV/atom,<sup>7</sup> equivalent to a material binding velocity of  $3.7044 \times 10^5$  cm/s. The value of  $\nu_b$  is  $.3163 \text{ cm}^{-1}$ , based on the Doppler shift formula

$$\nu_b = \left( \frac{V_b}{c} \right) \nu_0 . \quad (4)$$

Examples of Thompson fits to the measured Doppler profiles are given in Figs. 2 and 3, illustrating variations in distribution shape and magnitude over the field angle. Careful comparison of Figs. 2 and 3, with their common 550-eV beam energy, shows the considerable influence of the angle of incidence on Doppler profile and the differential and integrated sputter yield. Comparisons with common  $-30^\circ$  angle-of-incidence and differing beam energy reveal that integrated sputter yield at 250 eV is  $\sim$  one-third the yield at 550 eV for  $\theta_i = -30^\circ$ , as expected (see Figs. 4 and 5). The most probable kinetic energy of the sputtered particles lies between 2 and 6 eV in each case, approximately spanning the range  $E_b/2$  to  $E_b$ . The tail of the distribution extends well beyond 50 eV. For both sets of energy distributions shown (550 and 250 eV,  $\theta_i = -30^\circ$ , see Figs. 4 and 5), high  $\theta_f$  of  $45-75^\circ$  has the largest values for flux, tail amplitude and most probable energy, and low  $\theta_f$  of  $0^\circ$  or  $15^\circ$  has the smallest.

Figs. 6 and 7 show the variation of the parameter  $N$  of Eq. 1, in generating curve fits such as those of Figs. 2,3. The regular variation of  $N$  for  $\theta_i$  between 0 and  $-70$  deg. at 550 eV, spanning the range 2.2 to 3.7, provides strong evidence that fixing  $N$  constitutes a constraint that would reduce the quality of fit. Data fits with fixed  $N$  verified this situation, which is already obvious from Eq. 1; since we have fixed the value of  $\nu_b$  the equation only produces changes in Doppler profile through variation of  $N$ .

The variation of  $N$  at 550 eV exhibits a mostly decreasing trend as the emission angle increases and as ion incidence angle moves off normal, giving wider velocity distributions for those conditions (see Fig. 6), although for incidence far from normal  $N$  actually rises again at large  $\theta_f$ . Trends for 250-eV impingement energy are less apparent (see Fig. 7).

The most probable kinetic energies of the various Thompson curve fits, determined from measured Doppler shifts, are plotted in Figs. 8 and 9. As might be anticipated, plots of peak energy are very similar to the inverse variation of  $N$  (compare Figs. 6 and 8, and Figs. 7 and 9) and the variation of the Doppler width (full-width-half-maximum or FWHM) as plotted in Figs. 10 and 11. The peak energy usually occurs when  $\theta_f - \theta_i$  is approximately 90 degrees, for off-normal incidence, with  $\theta_i = -70$  and 550-eV impingement energy providing the main exception. The appearance of the peak energy curves in Figs. 8 and 9 depends strongly on impingement energy.

The relative density for the two beam energies is plotted in Figs. 12 and 13. For off-normal incidence, the peak density occurs where  $\theta_f - \theta_i$  is approximately 90 degrees. Normal incidence produces peak particle emission density at or near the surface normal, with less angular variation than observed for non-normal incidence. Since the velocity distributions do not vary dramatically, plots of the relative flux look similar to the relative density (see Figs. 14 and

15), so that the majority of the sputtered flux is directed toward the forward field angles. This phenomenon is much less prominent, or non-existent, at higher beam energies where the sputtered flux decreases with increasing field angle approximately as the cosine of the field angle.<sup>6</sup>

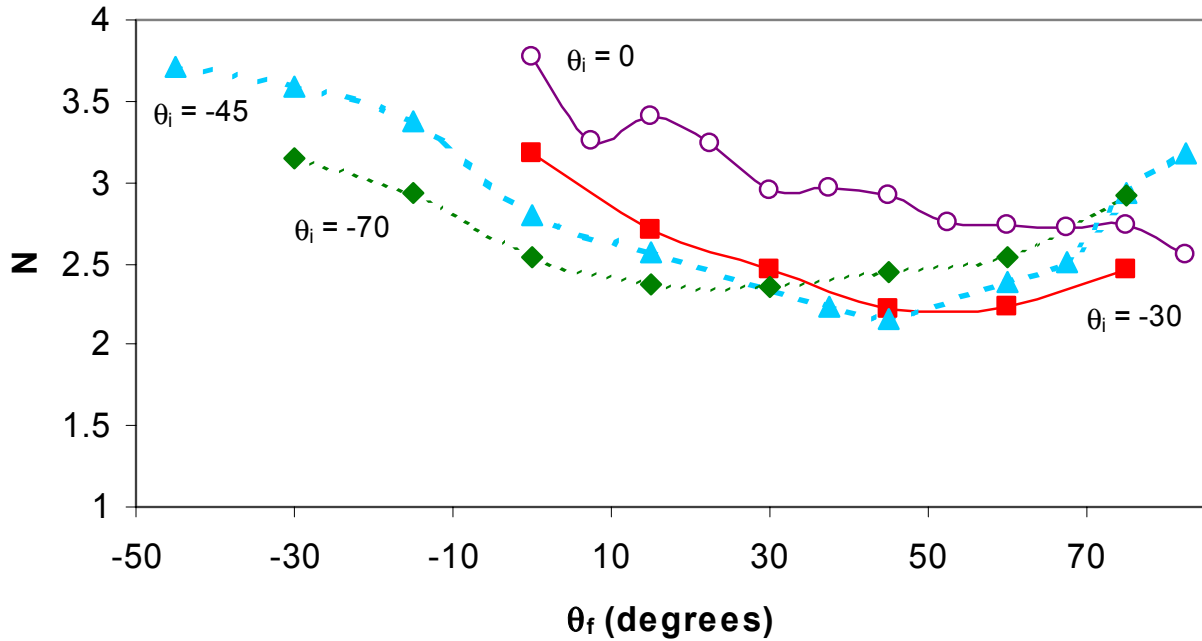


Figure 6. Thompson N-parameter variation with exit angle for 550-eV ion energy.

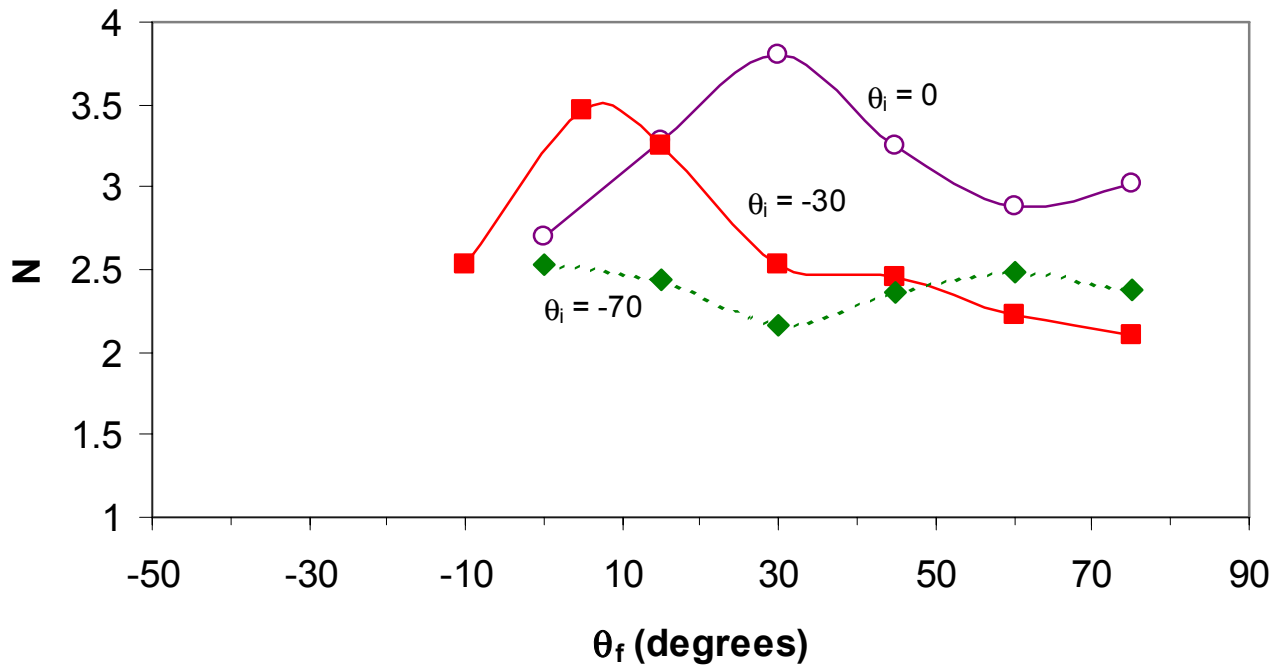


Figure 7. Thompson N-parameter variation with exit angle for 250-eV ion energy.

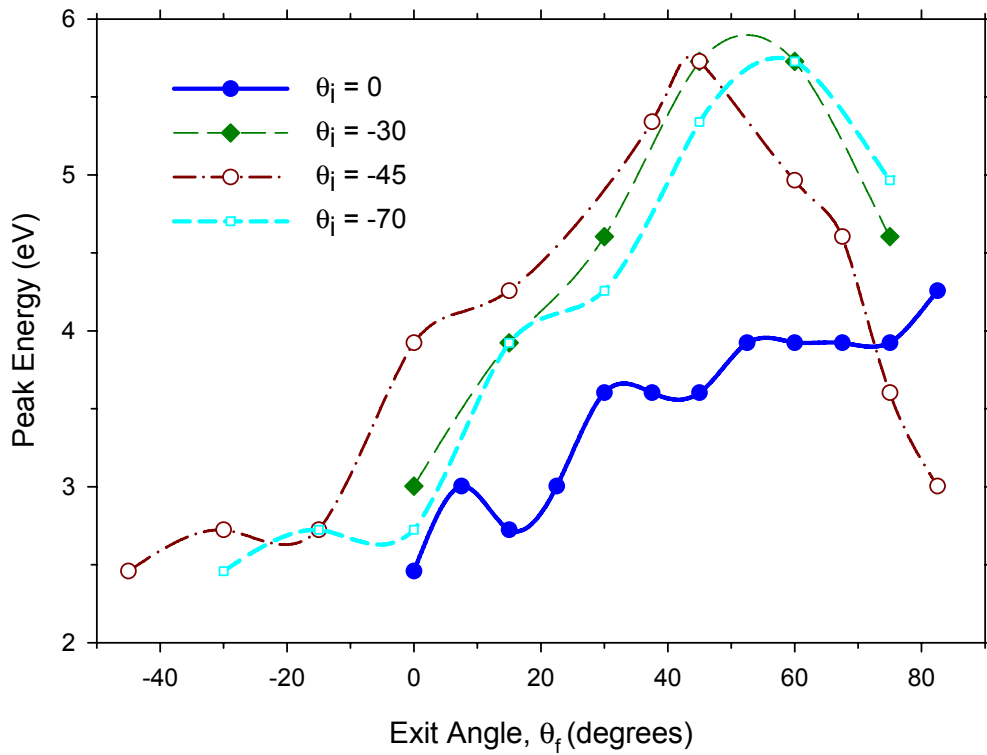


Figure 8. Peak kinetic energy of sputtered molybdenum vs. exit angle for 550-eV ion energy.

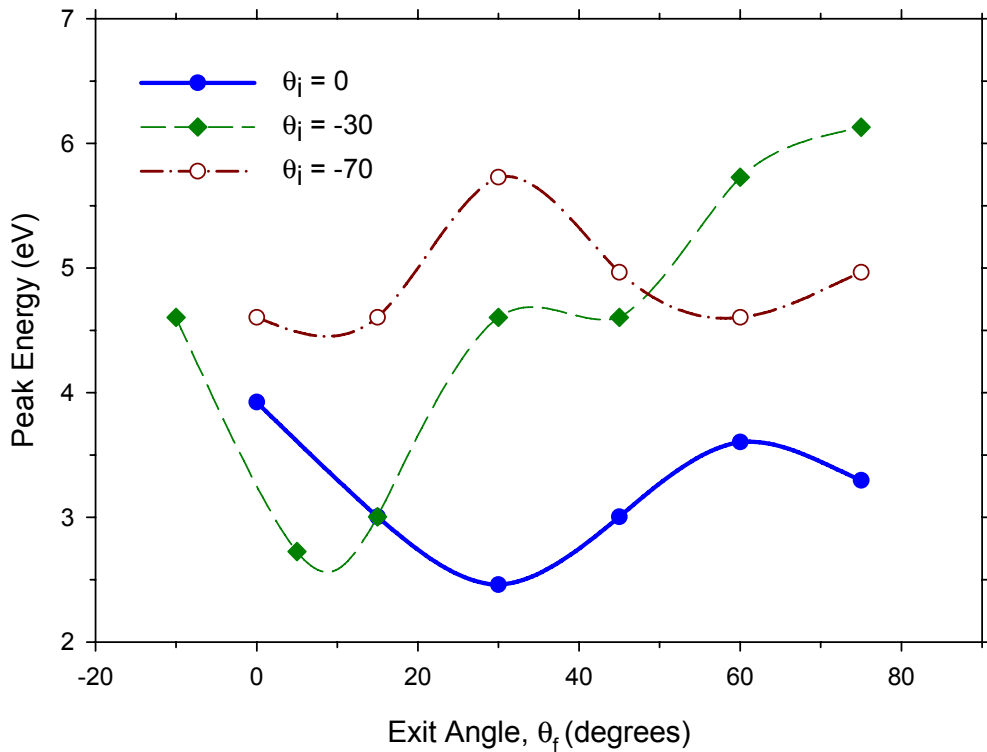


Figure 9. Peak kinetic energy of sputtered molybdenum vs. exit angle for 250-eV ion energy.

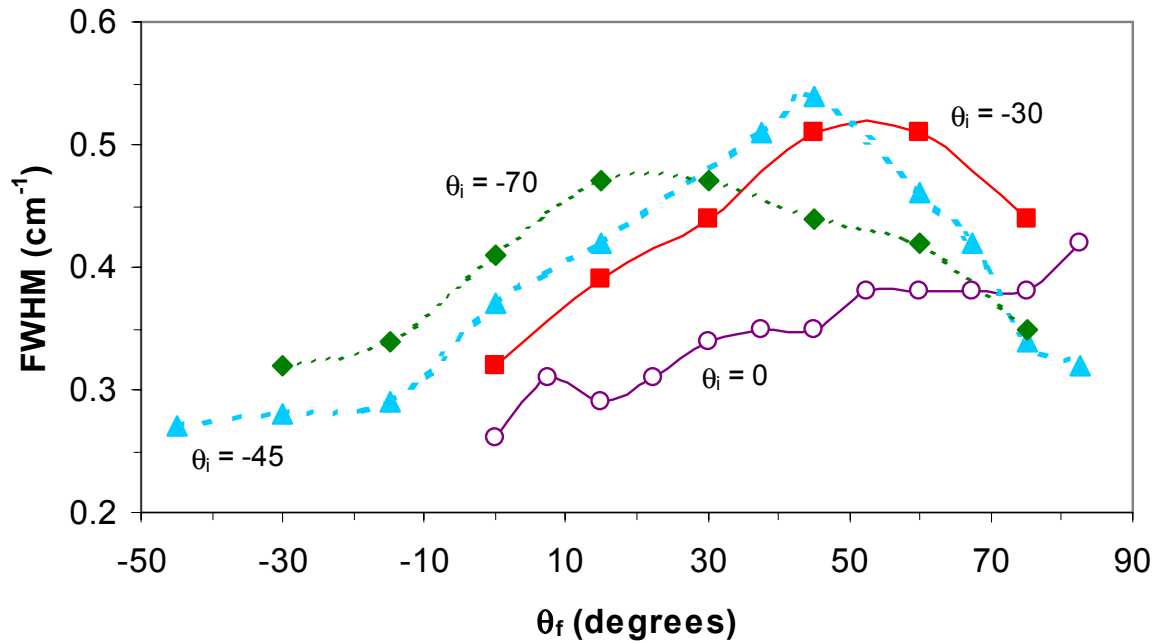


Figure 10. Width of sputtered molybdenum energy distributions vs. exit angle for 550-eV beam energy.

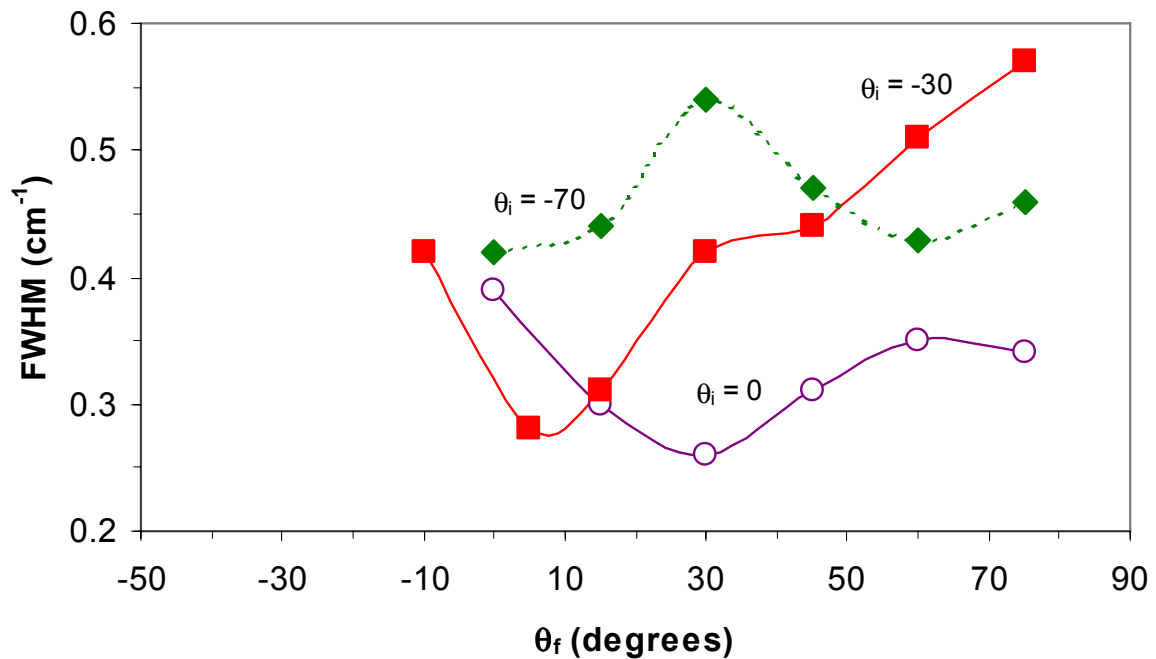


Figure 11. Width of sputtered molybdenum energy distributions vs. exit angle for 250-eV beam energy.

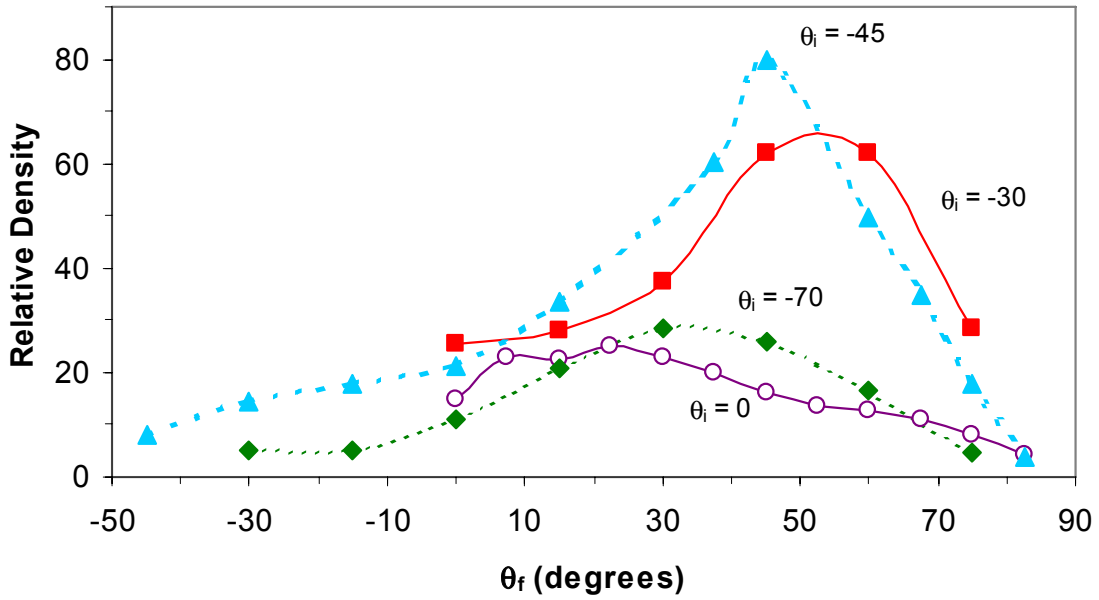


Figure 12. Sputtered molybdenum density vs. exit angle for 550-eV beam energy.

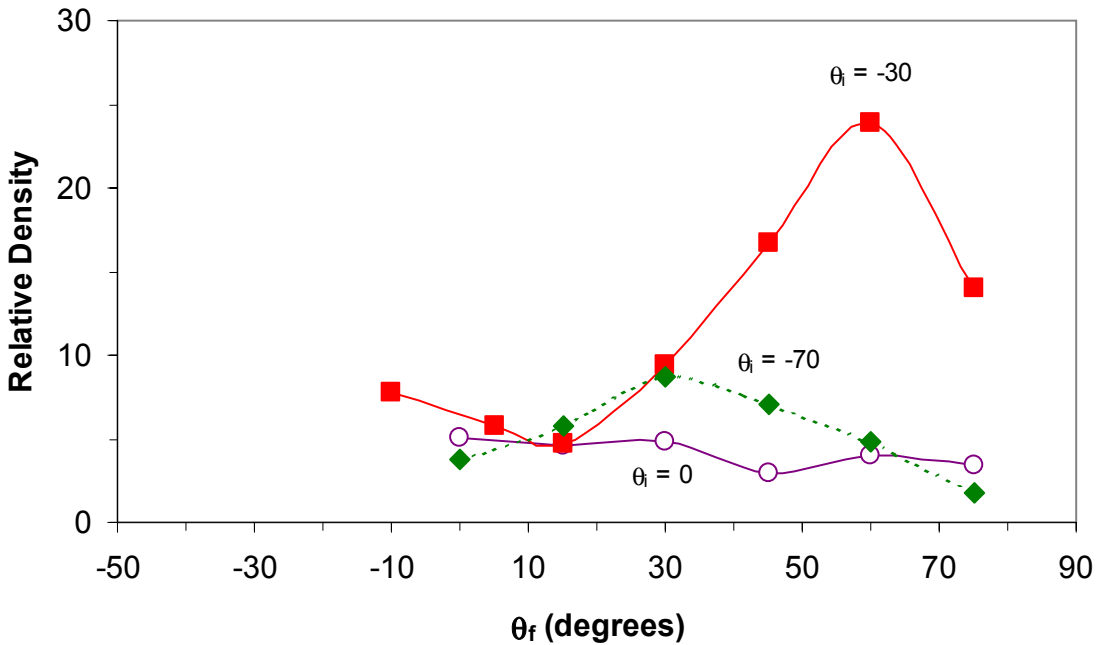


Figure 13. Sputtered molybdenum density vs. exit angle for a beam energy of 250 eV.

The absolute deposition rate measurements of the sputter flux generated from 1, 5, and 10-keV impingement, already mentioned,<sup>6</sup> are not sensitive to the energetics of the sputtered particles. However, they provide accurate differential and total sputter yields and, in principle, would allow the current LIF density and flux data to be converted to absolute numbers.

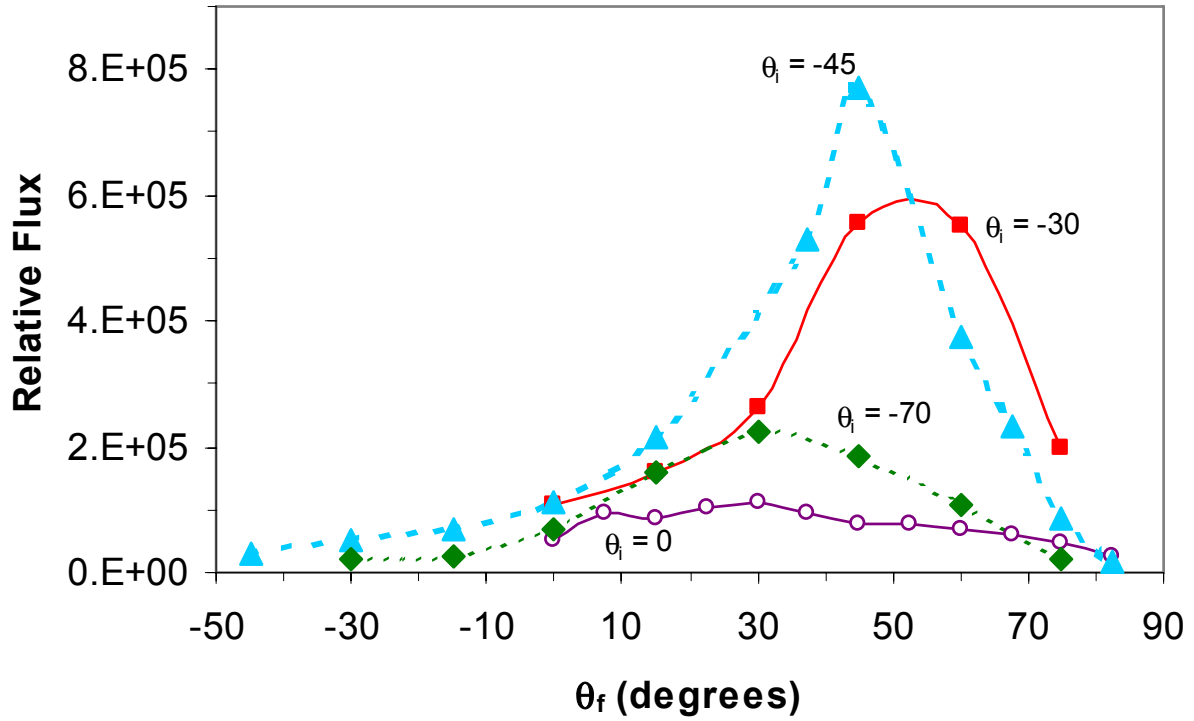


Figure 14. Relative particle flux vs. field angle for a beam energy of 550 eV.

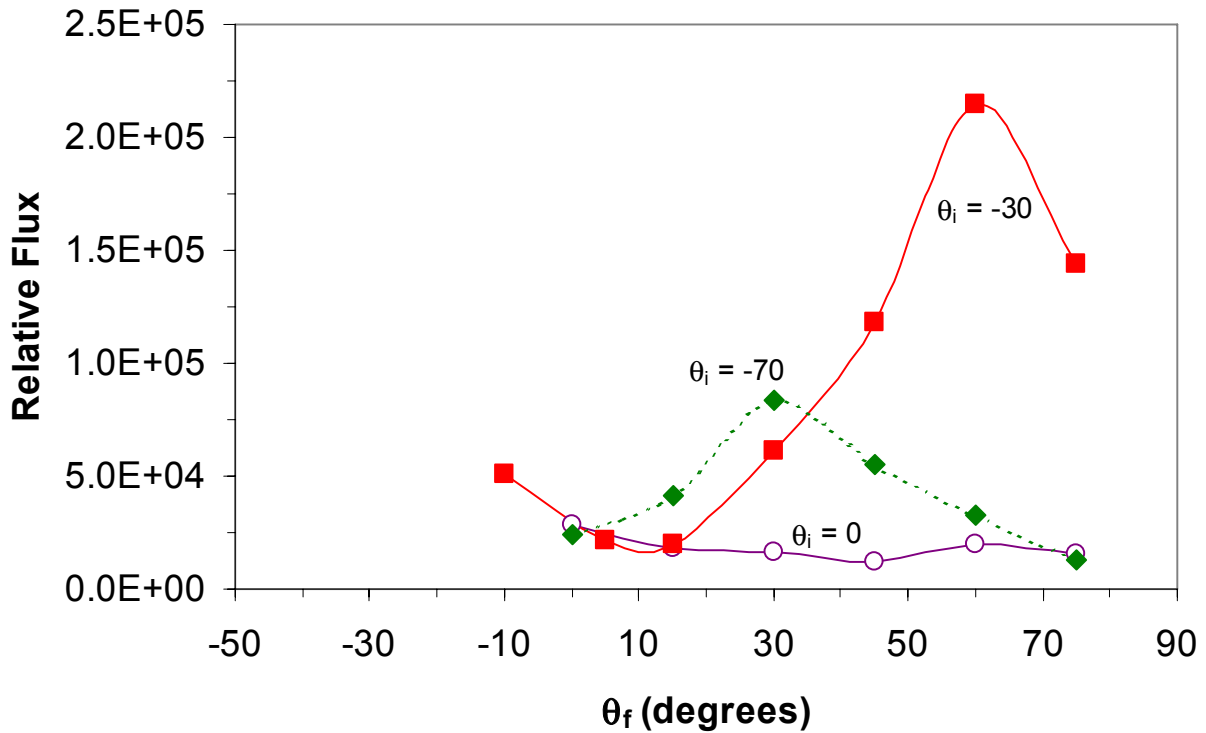


Figure 15. Relative particle flux vs. field angle for a beam energy of 250 eV.

#### IV. Concluding Remarks

The new results provide fundamental data at the highest level of detail, concerning xenon ion sputtering of molybdenum at low energy. The new information can be used for interpreting and quantifying molybdenum measurement data in ion engine plumes, and for the development of improved sputter and contamination models. Existing models generally assume a single molybdenum plume velocity and a constant or other simple (non-measured) density distribution. The high dependence of measured parameters, especially flux, on angles of incidence and observation, and the broad velocity/energy distributions that exist, indicate how approximate the current contamination and grid wear models are.

In a gridded ion engine, impingement on grid surfaces occurs over a broad distribution of incident angles and material is sputtered over a wide range of field angles. The distribution of incident energy varies from below the sputtering threshold to kV levels, an additional variable of high importance. Accurate modeling of erosion and re-deposition within the grid set and the computation of flux distribution about the thruster is therefore a complex problem requiring the very sort of data that was presented here. The experimental method is, in principle, applicable to the related problems of the angular flux distribution for ion-sputtered boron nitride and carbon-based materials.

The velocity distribution obtained at each incidence angle, field angle, and beam energy was fitted to a Thompson distribution. The parameter  $N$  had to be adjusted in each fit to achieve good results, since the observed velocity distribution varied significantly with angle and incident energy. These observations and the strong forward peaking behavior of the sputter flux demonstrate that linear-cascade collision conditions do not apply in the present study. A dramatic difference exists between the under-cosine or "butterfly" angular flux distributions found here, and the cosine or over-cosine distributions found at higher energy.

Comparisons between TRIM calculations and experimental results for this system reveal that the TRIM code does not work well under low energy, high angle conditions. Considerable room exists for improvements in fundamental understanding of low energy, high angle sputtering physics and models that would predict differential sputter yield behavior and other properties in these regimes.

#### Acknowledgments

Preparation of this manuscript was supported under The Aerospace Corporation's Independent Research and Development Program.

#### References

- <sup>1</sup>Behrisch R. and Wittmaack K., Sputtering by Particle Bombardment III (Springer-Verlag, 1991), *Topics in Applied Physics*, Vol. 64, 410 pp.
- <sup>2</sup>Gruen D.M., Pellin M.J., Young C.E. and Calaway, W.F., "Laser Spectroscopy of Sputtered Atoms," *J. Vac. Sci. Technol. A*, Vol. 4, No. 3, 1986, pp. 1779-1785.
- <sup>3</sup>Gaeta, C.J., Matossian, J.N., Turley R.S., Beattie J.R., Williams J.D., and Williamson W.S., "Erosion Rate Diagnostics in Ion Thrusters Using Laser-Induced Fluorescence," *J. Propulsion and Power* **9**, 369 (1993).
- <sup>4</sup>Crofton M.W., "Laser Spectroscopic Study of the T5 Ion Thruster," AIAA Paper 95-2921, 31<sup>st</sup> Joint Propulsion Conf., San Diego, July 1995.
- <sup>5</sup>Ahmed L.N. and Crofton M.W., "Surface Modification Measurements in the T5 Ion Thruster Plume," *J. Propulsion and Power*, Vol. 14, No. 3, 1998, pp. 336-347.
- <sup>6</sup>Williams J.D., Gardner M.M., Johnson M.L. and Wilbur P.J., "Xenon Sputter Yield Measurements for Ion Thruster Materials," Paper 03-130, 28<sup>th</sup> International Electric Propulsion Conference, Toulouse, Mar 2003.
- <sup>7</sup>NIST webbook, (<http://physics.nist.gov/cgi-bin/AtData/display.ksh?XXE0qMoqIXXP-15XXT2XXS>)
- <sup>8</sup>Thompson, M.W., *Phys. Rep.*, Vol. 69, 1981, p. 335.
- <sup>9</sup>Husinsky W., Girgis I. and Betz G., "Doppler Shift Laser Fluorescence Spectroscopy of Sputtered and Evaporated Atoms under Ar+ Bombardment," *J. Vac. Sci. Technol. B*, Vol. 3, No. 5, 1985, pp. 1543-1545.
- <sup>10</sup>Goehlich A., Rowekamp M. and Dobeles, H.F., "Determination of the Velocity Distribution of Sputtered Atomic Oxygen by Laser-Induced Fluorescence in the Vacuum-Ultraviolet (130 nm)," *Surf. Sci.*, Vol. 248, 1991, pp. 271-275.
- <sup>11</sup>Stuart R.V., Wehner G.K. and Anderson G.S., "Energy Distribution of Atoms Sputtered from Polycrystalline Metals," *J. Appl. Phys.*, Vol. 40, No. 2, 1969, pp. 803-812.
- <sup>12</sup>Wright R.B., Young C.E., Pellin M.J. and Gruen D.M., "High Resolution Continuous Wave Laser Induced Fluorescence Spectroscopy of Sputtered Zr Atoms," *J. Vac. Sci. Technol.*, Vol. 20, No. 3, 1982, pp. 510-514.
- <sup>13</sup>Miotello A. and Kelly R., "On the Origin of the Different Velocity Peaks of Particles Sputtered from Surfaces by Laser Pulses or Charged-Particle Beams," *Appl. Surf. Sci.*, Vol. 138, 1999, pp. 44-51.